The vibroacoustic interaction in mallet percussion instruments: modelling and experiments

Filipe Soares[1], Vincent Debut[1,2,3], Jose Antunes[1,2]

[1] Instituto Superior Técnico - Centro de Ciências e Tecnologias Nucleares, Portugal

[2] Instituto de Etnomusicologia, Centro de Estudos em Música e Dança Universidade Nova de Lisboa, Portugal

[3] Instituto Politécnico de Castelo Branco Escola Superior de Artes Aplicadas, Portugal

PACS: 43.75

Resumen

En algunos instrumentos de percusión de mazo, como vibráfonos y marimbas, se colocan resonadores acústicos debajo de las barras afinadas para mejorar la radiación acústica. Aunque se utiliza mucho en instrumentos comerciales, la interacción vibro-acústica entre las barras afinadas y sus resonadores no se ha estudiado de forma exhaustiva, y los intentos de modelado anteriores suelen descuidar aspectos importantes de la dinámica de acoplamiento. Este trabajo se basa en un estudio previo, donde se presentó un modelo mínimo para el acoplamiento entre un único modo de barra y un único modo de resonador. Aquí, los mismos principios de modelado se aplican a un sistema compuesto por una barra 1-D y un resonador acústico cilíndrico, llevando a un modelo simplificado que incluye la dinámica de acoplamiento entre varios modos de barra y varios modos acústicos de resonador. La dinámica del modelo se explora a través de simulaciones en el dominio temporal y análisis de valores propios, revelando una serie de características interesantes, por ejemplo: el papel de la relación de coeficientes de amortiguamiento entre un modo de barra y un modo de resonador, la colocación del resonador a longo de la barra, así como su proximidad a la barra. Además, se presentan resultados experimentales para validar el modelo y demostrar su capacidad para emular instrumentos reales, tanto cualitativa como cuantitativamente.

Palabras clave: interacción barra-resonador, acoplamiento vibroacústico, modelado simplificado, validación experimental.

Abstract

In some mallet percussion instruments, such as vibraphones and marimbas, tubular acoustic resonators are placed beneath the tuned bars to enhance sound radiation. Although widely used in commercial instruments, the vibroacoustic interaction between the tuned bars and their resonators has not been studied extensively, and previous modelling attempts regularly neglect important aspects of the coupling dynamics. This work develops on a previous study, where a minimal model for the coupling between a single bar mode and a single resonator mode was presented. Here, the same modelling principles are applied to a system composed of a 1-D beam and a 1-D cylindrical acoustic resonator, leading to a lumped-parameter model including the coupling dynamics between several bar modes and several resonator acoustic modes. The dynamics of the lumped-parameter model are explored through time-domain simulations and eigenvalue analysis, reveling a number of interesting (and rarely mentioned) features, for example: the role of the ratio of damping coefficients between a bar mode and a resonator mode, the placement of the resonator along the bar's length as well as its proximity to the bar, etc. Additionally, experimental results are presented to validate the model and demonstrate its capacity to emulate real instruments, both qualitative and quantitatively.

Keywords: bar-resonator interaction, vibroacoustic coupling, simplified modelling, experimental validation.

1. Introduction

Mallet percussion instruments (e.g. marimba, vibraphone, xylophone, etc.) are made of various tuned bars that vibrate and radiate sound at their natural frequencies of vibration. The tuning process involves cutting on the underside of the bars such that their frequencies become harmonically aligned (multiple integers of the fundamental frequency). Recent years have seen a number of studies [1] [2] [3] [4] using optimization methods to find undercut

geometries that lead to the tuning of multiple bar modes to a set of predefined targets. Moreover, some studies considered the concomitant tuning of non-vertical-bending modes (torsional, lateral) with vertical-bending modes [5] [6].

In some instruments, resonator pipes are used to enhance sound radiation. Early experimental reports by Bork [7] have demonstrated that when the fundamental frequency of the acoustic resonator is aligned with that of a bar mode, the two (mechano-acoustic) elements experience a vibro-acoustic coupling, which generally leads to an increase of sound radiation. On the other hand, the increased sound radiation is often accompanied by a proportional decrease of the bar decay time.

Despite the advances on the design optimization of the individual elements (bars and resonators), the nature of the vibro-acoustic coupling between the two has not been studied extensively. To the authors knowledge, the only work dealing with the two-way coupling is that recently published by Rucz et al. [8]. Here, the authors use 3-D finite element models to describe the vibroacoustic coupling between cylindrical resonators and bars and, in general, their numerical results are in agreement with experiments, expressing both the increase in sound radiation and the decrease of bar decay time. However, approaches using 3-D models entail large computational costs and are less practical for parametric studies. In this context, simplified modelling approaches may be useful in underlining the main parameters influencing the instruments' behavior.

In recent work by the authors [9] [10], a simplified model for the vibro-acoustic interaction was developed. To this end, a single bar mode was represented by a disk-shaped damped oscillator, and the acoustics of a cylindrical resonator (of the same radius) were described in a modal framework. The vibro-acoustic transfer function between the two elements was calculated via a 2-D axisymmetric finite element model, whose numerical results were then fitted to dimensionless analytical expressions. Finally, the interaction between a single bar mode and a single resonator mode was reduced to a system of two coupled oscillators. Despite its simplicity, the model was able to reproduce the dynamical behavior commonly observed in experimental reports.

In this work we develop on the previous modelling efforts, now including the interaction between multiple bar and resonator modes. Subsequently, several experimental investigations are carried out to validate various aspects of the proposed model, and assess its capacity to describe the dynamics of real instruments, both qualitatively and quantitatively.

2. Model description

We consider the coupling dynamics between a free-free vibrating beam and a cylindrical acoustic waveguide, as illustrated in Figure 1. The resonator is closed at the bottom and open (unflanged) at the top. The beam has length L_B and its width is equivalent to the resonator diameter ($2a$). The resonator is located at a distance x_e along the beam length and its open termination is located at a distance d below the bar.

2.1. Dynamics of the uncoupled bar

The linear dynamics of a beam with free-free boundary conditions are described in a modal framework, that is

$$m_n\ddot{\alpha}_n(t)+2m_n\zeta_n\omega_n\dot{\alpha}_n(t)+m_n\omega_n^2\alpha_n(t)=0 \qquad (1)$$

for $n=1, 2 \ldots N$, where m_n, ζ_n, ω_n and $\alpha_n(t)$ are the modal masses, damping ratios, natural frequencies and participation factors of the beam modes, respectively, and the beam vertical displacement $Y(x,t)$ is given by the sum of the modal contributions

$$Y(x,t)=\sum_{n}^{N}\psi_n(x)\alpha_n(t) \qquad (2)$$

where $\psi_n(x)$ are the beam mode shapes.

2.2. Acoustics of the uncoupled resonator

The acoustic wave equation in terms of particle displacement $w(y,t)$ is given by the following partial differential equation

$$\rho S\left(\frac{1}{c^2}\frac{\partial^2 w(y,t)}{\partial t^2}-\frac{\partial^2 w(y,t)}{\partial y^2}\right)=0 \qquad (3)$$

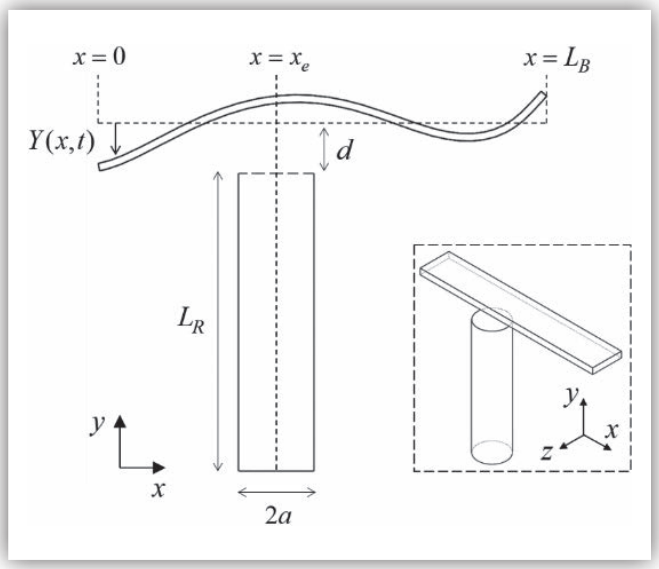

Figure 1. Illustrative diagram of the considered model.

where ρ is the fluid density at rest, c is the speed of sound and S is the cross-sectional area of the pipe. At the closed end $y = 0$, there is no displacement and the boundary condition is $w(0,t) = 0$, while at the open end $y = L_R$, we impose a radiation impedance Z_R such that the pressure $p(L_R,t)$ and fluid velocity $u(L_R,t)$ obey the following relation, in the Laplace domain,

$$Z_R(s) = \frac{p(L_R,s)}{u(L_R,s)} = \rho c(s^2 R_R + sX_R) \tag{4}$$

where s is the complex Laplace variable; R_R and X_R are associated to the acoustic resistance and reactance, respectively. In terms of particle displacement, the boundary condition at the open-end $y = L_R$ is written as

$$\frac{-\int w(y,s)dy\Big|_{y=L_R}}{w(L_R,s)} = c(sR_R + X_R) \tag{5}$$

Replacing the two boundary conditions into the wave equation (3) eventually leads to the pipe's characteristic equation

$$\coth\left(\frac{sL}{c}\right) + s^2 R_R + sX_R = 0 \tag{6}$$

whose solutions s_r are the complex eigenvalues of the uncoupled resonator. Solutions can be found numerically to obtain the real and imaginary parts of the eigenvalues $s_r = a_r + jb_r$, from which the undamped natural frequencies $\underline{\omega}_r$ and damping ratios $\underline{\zeta}_r$ of each acoustic mode r can be obtained. Then, we can develop the particle displacement $w(y,t)$ in terms of the (real) acoustics modes $\phi_r(y)$ as

$$w(y,t) = \sum_{r=1}^{R} \phi_r(y)\gamma_r(t), \text{ where } \phi_r(y) = \sin\left(\frac{\underline{\omega}_r}{c} y\right) \tag{7}$$

Substitution of (7) into the wave equation (3) and proceeding with the typical Galerkin projection leads to a system where, in general, orthogonality does not strikly hold. However, it can be shown that for pipes that are not unreasonably wide $(a/L < 0.1)$, the contributions of off-diagonal terms are small and the following (orthogonal) approximation is suitable

$$\int_0^L \phi_n(x)\phi_m(x)dx \approx \begin{cases} \dfrac{L+\Delta L}{2} & \text{for} \quad m = n \\ 0 & \text{for} \quad m \neq n \end{cases} \tag{8}$$

where ΔL is the length correction term ($\Delta L = X_R c$). Finally, using (8), eventually leads to a set of (linearly independent) modal equations describing the resonator acoustics

$$\underline{m}_r \ddot{\gamma}_r(t) + 2\underline{\zeta}_r \underline{m}_r \underline{\omega}_r \dot{\gamma}_r(t) + \underline{m}_r \underline{\omega}_r^2 \gamma_r(t) = 0 \tag{9}$$

for $r = 1,2...R$, where the inertial modal coefficients $\underline{m}_r$ are given by $\underline{m}_r \simeq \rho S(L + \Delta L)/2$.

2.3. Vibroacoustic interaction

A difficult aspect in modelling the interaction between a vibrating bar and its acoustic resonator is associated with the three-dimensional effects of the acoustic radiation that couple the two elements. Here, we simplify the geometry of the problem by assuming that only a particular region in the beam surface will have a meaningful vibro-acoustic interaction with the resonator. Namely, we consider the circular area on the beam that is located directly above the open end of the resonator, as illustrated in Figure 2.

The vibro-acoustic coupling is defined by the interaction between the motion of disk (beam) and the acoustics at the open end of the resonator. On this point, we remind the reader of the principle of vibro-acoustical reciprocity [11] [12]. In our problem, this principle can be arranged in the form of a dimensionless transfer function H

$$H(\omega) = \frac{F_r(x_e,\omega)}{p(L_R,\omega)S} = \frac{\dot{Q}_b(L_R,\omega)}{\ddot{Y}(x_e,\omega)} \tag{10}$$

where $\dot{Q}_b(L_R,\omega)$ is an acoustic volume acceleration induced on the resonator open-end by the beam-disk motion and, similarly, $F_r(x_e,\omega)$ is the net force induced on the beam-disk by the acoustic radiation from the open-end of the resonator. In a recent work [9] [10] this transfer function was numerically calculated via a 2-D axisymmetric finite element model considering the interaction between two parallel circular surfaces of the same radius a, for various separation distances d/a. It was found that, in the low-frequency range ($ka < 1$), the transfer function $H(ka, d/a)$ can be approximated by a simple constant gain filter, dependent solely on the dimensionless dis-

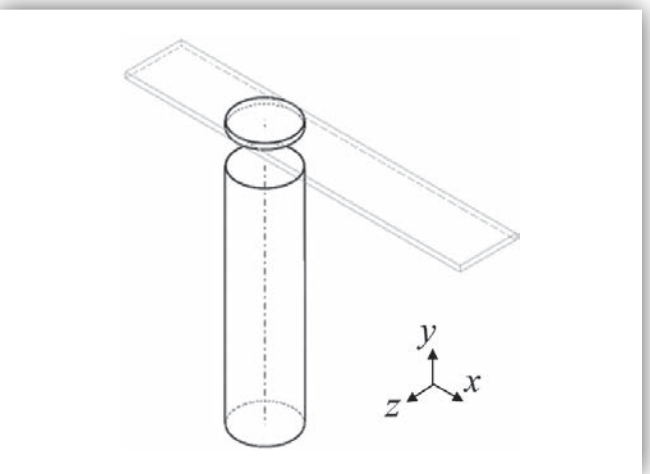

Figure 2. Illustration of the portion of the beam considered in the vibro-acoustic interaction.

tance d/a. The numerical results were fitted to a polynomial function of the following form

$$H(d/a)=\left(1+\sum_{p=1}^{P}\delta_p\left(\frac{d}{a}\right)^p\right)^{-1} \tag{11}$$

considering various orders P. A 5th-order polynomial was deemed sufficient for an accurate description of the calculate transfer function, leading to the fitted coefficients $\delta_p=[2.78,-1.03,3.34,-1.15,0.13]$. Notice that, when $d\to 0\Rightarrow H\to 1$ and when $d\to\infty\Rightarrow H\to 0$, as expected. Finally, with the knowledge of $H(d/a)$, the force $F_r(x_e,t)$ and the acoustic excitation $\dot{Q}_b(L_R,t)$ can be used as forcing terms in the equations of the beam (1) and of the resonator (9), respectively.

2.4. Coupled system

Given the vibro-acoustic transfer function (11), the force load on the beam-disk induced by the resonator is then given by

$$F_r(x,t)=-\delta(x-x_e)\rho SH(d/a)\sum_{r=1}^{R}\ddot{\gamma}_r(t)\varphi_r(L_R) \tag{12}$$

where the auxiliary function (associated with the resonator mode shapes in terms of pressure) is

$$\varphi_r(y)=\int\phi_r(y)dy=-\left(\frac{c}{\underline{\omega}_r}\right)\cos\left(\frac{\underline{\omega}_r}{c}y\right) \tag{13}$$

Projection unto the beam modal basis $\psi_n(x)$ will yield the modal forces $F_n(t)$ applied on each beam mode which eventually lead to the beam modal equations

$$\begin{aligned}m_n\ddot{\alpha}_n(t)+2m_n\omega_n\zeta_n\dot{\alpha}_n(t)+m_n\omega_n^2\alpha_n(t)=\ldots\\ \ldots\rho SH(d/a)\psi_n(x_e)\sum_{r=1}^{R}\varphi_r(L_R)\ddot{\gamma}_r(t)\end{aligned} \tag{14}$$

Similarly, the volume acceleration induced on the resonator by the beam-disk motion is given by

$$\dot{Q}_{sr}(L_R,t)=SH(d/a)\ddot{Y}(x_e,t) \tag{15}$$

which can be used as a forcing term in the (inhomogeneous) wave equation. Following the appropriate Galerkin projection unto the acoustic modal basis, the resonator modal equations are

$$\begin{aligned}\underline{m}_r\ddot{\underline{\gamma}}_r(t)+2\underline{m}_r\underline{\omega}_r\underline{\zeta}_r\dot{\underline{\gamma}}_r(t)+\underline{m}_r\underline{\omega}_r^2\underline{\gamma}_r(t)=\ldots\\ \ldots-\rho SH(d/a)\varphi_r(L_R)\sum_{n=1}^{N}\psi_n(x_e)\ddot{\alpha}_n(t)\end{aligned} \tag{16}$$

The final coupled system is then described by a series of N (mechanical) oscillators inertially coupled to R (acoustic) oscillators

$$\begin{aligned}&\begin{bmatrix}M_n & \Pi_{n,r}\\ \Pi_{r,n} & M_r\end{bmatrix}\begin{Bmatrix}\ddot{\alpha}_n\\ \ddot{\gamma}_r\end{Bmatrix}+\begin{bmatrix}C_n & 0\\ 0 & C_r\end{bmatrix}\begin{Bmatrix}\dot{\alpha}_n\\ \dot{\gamma}_r\end{Bmatrix}\ldots\\ &\ldots+\begin{bmatrix}K_n & 0\\ 0 & K_r\end{bmatrix}\begin{Bmatrix}\alpha_n\\ \gamma_r\end{Bmatrix}=\begin{Bmatrix}0\\ 0\end{Bmatrix}\end{aligned} \tag{17}$$

where the modal sub-matrices M_b, C_b, K_b, M_r, C_r and K_r, are diagonal and define the modal parameters of the beam and resonator, i.e.

$$\begin{aligned}&\mathrm{diag}(M_n)=m_n && ;\ \mathrm{diag}(M_r)=\underline{m}_r\\ &\mathrm{diag}(C_n)=2\zeta_n m_n\omega_n && ;\ \mathrm{diag}(C_r)=2\underline{\zeta}_r\underline{m}_r\underline{\omega}_r\\ &\mathrm{diag}(K_n)=m_n\omega_n^2 && ;\ \mathrm{diag}(K_r)=\underline{m}_r\underline{\omega}_r^2\end{aligned} \tag{18}$$

while the elements in the inertial coupling matrix are given by

$$\Pi_{n,r}=\rho SH(d/a)\varphi_r(L_R)\psi_n(x_e) \tag{19}$$

2.5. Energy balance

The kinetic and potential modal energies in each beam mode are given by

$$T_n(t)=\frac{m_n}{2}\dot{\alpha}_n^2(t)\quad ;\quad U_n(t)=\frac{m_n\omega_n^2}{2}\alpha_n^2(t) \tag{20}$$

Similarly, the acoustic kinetic and potential modal energies in each resonator mode are

$$\underline{T}_r(t)=\frac{\underline{m}_r}{2}\dot{\underline{\gamma}}_r^2(t)\quad ;\quad \underline{U}_r(t)=\frac{\underline{m}_r\underline{\omega}_r^2}{2}\underline{\gamma}_r^2(t) \tag{21}$$

The amount of energy dissipated by each beam mode, via internal losses, is given by

$$D_n(t)=2\zeta_n m_n\omega_n\int_0^t\dot{\alpha}_n^2(\tau)d\tau \tag{22}$$

while the amount of energy dissipated by each resonator mode, through acoustic radiation, is given by

$$\underline{D}_r(t)=2\underline{\zeta}_r\underline{m}_r\underline{\omega}_r\int_0^t\dot{\underline{\gamma}}_r^2(\tau)d\tau \tag{23}$$

The energy conserved in a given (coupled) modal-pair nr is given by

$$E_{C,nr}(t)=U_n(t)+T_n(t)+\underline{U}_r(t)+\underline{T}_r(t) \tag{24}$$

Additionally, we define a "modal radiation efficiency" κ_{nr}, representing the percentage of energy in the modal-pair nr nr that is dissipated through acoustic radiation by a resonator mode

$$\kappa_{nr}=\frac{\underline{D}_r(t\to\infty)}{E_{T,nr}}\times 100\% \tag{25}$$

where $E_{T,nr}$ is the total energy in the modal pair. We also define the decay time of the coupled modal-pair $T_{60,nr}$ as

$$T_{60,nr} \Rightarrow \frac{E_{C,nr}(T_{60,nr})}{E_{C,nr}(0)} = 0.001 \qquad (26)$$

3. Experimental validation

To assess the validity of the proposed vibro-acoustic model, an experimental apparatus was set-up in an anechoic chamber. The aim was to evaluate the behavior of the coupled-system, both qualitatively and quantitatively, in terms of the most pertinent design parameters: tuning ratio $\underline{\omega}_r/\omega_n$, the bar-resonator distance d and the resonator placement along the bar length x_e.

As illustrated in Figure 3, the set-up was made of a suspended beam placed over a cylindrical pipe of variable length. The pipe inner radius was $a = 25$ mm, and it was composed of two parts joint by a threaded junction, which allowed for a precise variation of its overall length $(440\text{ mm} \le L_R \le 530\text{ mm})$. The acoustic response of the pipe was measured by an electret microphone placed at the bottom end. The used aluminum beam was suspended by elastic strings on a tri-pod mount, which allowed the control of the bar-resonator distance d. The bar length was $L_B = 350$ mm and its width equal to the tube diameter $2a$. The beam was undercut (based on [6]) such that its first four vertical-bending modes are tuned in a ratio (1:3:5:7) and its flat surface was faced down to ensure the distance d was constant along the beam length. The beam was given an impulsive excitation with a small impact hammer (Brüel & Kjær – Type 8203) striking at one end ($x \approx L_B$), while its motion was measured at the other end ($x \approx 0$) using a laser vibrometer (Polytech – PDV100).

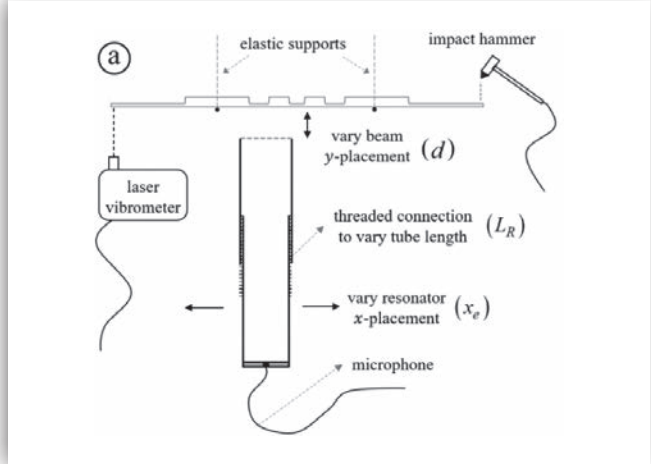

Figure 3. Diagram of the experimental set-up for the study of the vibroacoustic interaction.

3.1. Experimental modal identification

Since the aim was to experimentally validate the proposed model, the first step was the modal identification of the bar and resonator modes, such that identified modal parameters could be used in the model for comparison. The first four vertical-bending modes of the bar and the first four resonator acoustics modes were identified, for several tube lengths L_R. The identified modal parameters are shown in Table 1.

The parameters of the resonator are shown in ranges, corresponding to the variations in resonator length. Additionally, Figure 4 shows the profile of the undercut bar as well as the first four mode shapes $\psi_n(x)$. The considered modal masses $(m_n, \underline{m}_r)$ and mode shapes $(\psi_n(x), \phi_r(y))$ were taken from models as these parameters are not particularly easy to measure experimentally and small quantitative differences compared to the modelled values are not expected to change results significantly.

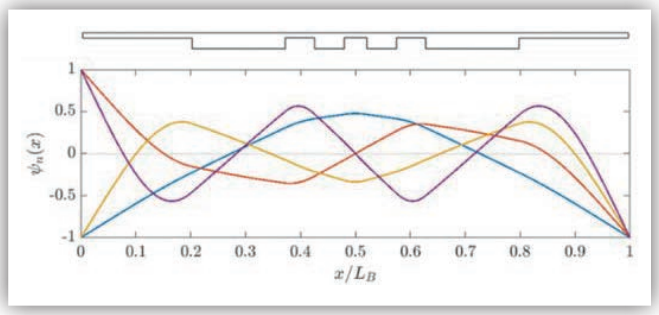

Figure 4. Profile of the undercut bar (top) and considered modes shapes $\psi_n(x)$.

Table 1. Modal parameters for the first four bar and resonator modes.

	Bar			Resonator		
n, r	$\omega_n/2\pi$ (Hz)	ζ_n (%)	m_n (kg)	$\underline{\omega}_r/2\pi$ (Hz)	$\underline{\zeta}_r$ (%)	$\underline{m}_r$ (g)
1	168.7	0.042	0.045	173.7 ± 12.5	0.73 ± 0.04	0.61± 0.04
2	505.1	0.024	0.031	507.6 ± 32.8	0.77 ± 0.04	0.61± 0.04
3	847.7	0.022	0.024	845.1 ± 56.8	0.83 ± 0.06	0.61± 0.04
4	1186	0.009	0.037	1205.9 ± 78.6	0.94 ± 0.08	0.61± 0.04

3.2. Effect of tuning ratio and beam-resonator distance

In the first set of measurements, the aim was to measure the decay time $T_{60,nr}$ and "radiation efficiency" κ_{nr} of different modal pairs as a function of the tuning ratio $\underline{\omega}_r/\omega_n$. The resonator was maintained centered with the bar $x_e = L_B/2$, and measurements were taken for a sweep of discrete tube lengths such that $0.95 \leq \underline{\omega}_r/\omega_n \leq 1.05$. Since the bar frequencies are tuned to a ratio close to that of the resonator (1:3:5:7), this procedure allowed for the measurement of all four modal-pair couplings at the same time. Additionally, in order to quantitatively validate the proposed vibro-acoustic transfer function $H(d/a)$, this procedure was repeated for three bar-resonator distances $d = [10 \;\; 20 \;\; 40]$ mm. Results for the coupling in first and third modal pairs are shown in Figure 5. Note that with $x_e = L_B/2$, the coupling of the second and fourth bar modes is bound to be weak since $\psi_2(x_e) = \psi_4(x_e) = 0$. For these modal pairs, results showed no significant variation of the time decay $T_{60,nr}$ compared to the uncoupled case, and resonator dissipation K_{nr} was negligible ($K_{nr} < 0.5\%$, for all $\underline{\omega}_r/\omega_n$). Results in Figure 5 demonstrate that, qualitatively, the model is able to predict the observed behavior, with the typical decrease in decay time being accompanied by a proportional increase in resonator damping. Moreover, the decrease in coupling strength when the bar is placed further away (larger d/a) is also captured by the model. However, quantitatively, the model seems to underestimate the coupling strength in all cases: the decrease in time decays $T_{60,nr}$ and increase in resonator damping K_{nr} is always larger in the experimental results. This difference can potentially be attributed to the fact that our vibro-acoustic coupling is based on the disk geometric simplification, whereby in reality, other regions of the beam will also couple with the resonator acoustics.

3.3. Effect of resonator placement

In this second series of experiments, the distance was fixed at $d/a = 0.4$, and the resonator length was fixed such that $\underline{\omega}_r/\omega_n \approx 1$, for each modal-pair. Then, a series of measurements were performed for a sweep of discrete resonator placements in the region $0.5 \leq x_e/L_B \leq 1$. Due to bar symmetry, only half the domain was mapped. Results for the decay time $T_{60,nr}$ and resonator dissipation K_{nr} are shown in Figure 6. In general, modelling results agree well with the observed behavior, where we see a significant decrease in the coupling strength when the resonator is placed below a nodal line of the bar mode $(\psi_n(x_e) = 0)$ (see Figure 4). We also note a slight difference in the shapes of the $T_{60,nr}$ and K_{nr} curves, likely due to small differences between the considered and actual mode shapes of the beam. Finally, we notice large differences when the resonator is placed near the tip of the bar $0.95 \leq x_e/L_B \leq 1$, in all cases. This deviation is expected since, in these scenarios, the bar does not cover the resonator termination completely (for example, when $x_e/L_B = 1$, the bar only covers half the resonator open-end). Here, the disk-assumption naturally leads to an overestimation of the coupling strength.

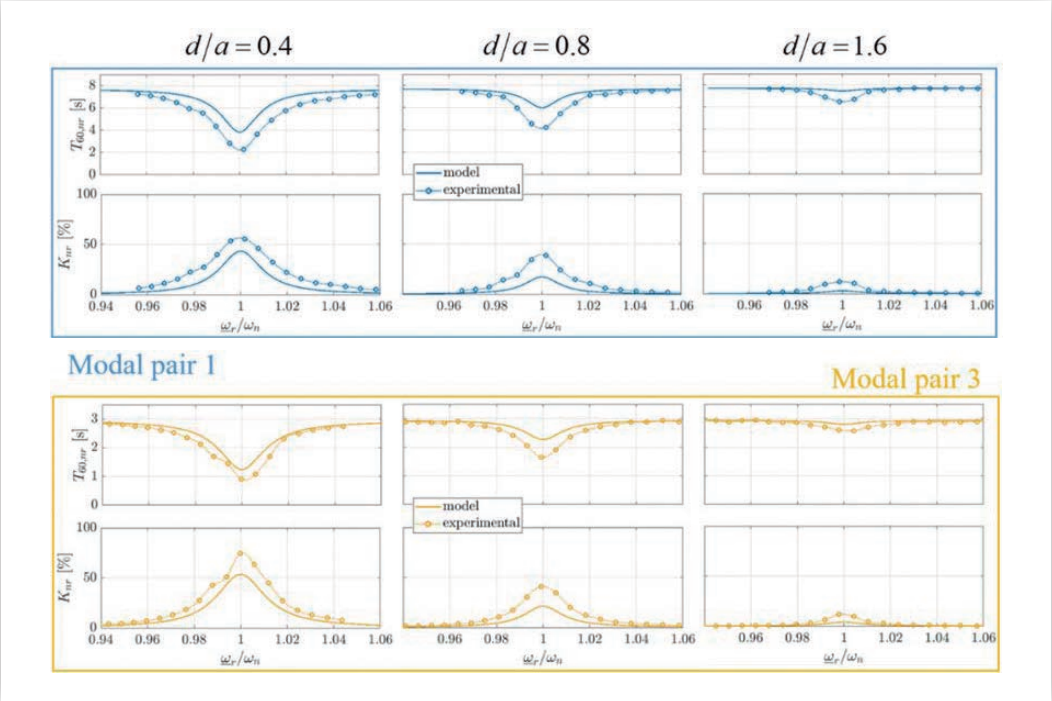

Figure 5. Variation of the decay time $T_{60,nr}$ (s) and resonator dissipation K_{nr} (%) as a function of the tuning ratio $\underline{\omega}_r/\omega_n$, for three different bar-resonator distances $d = [10 \;\; 20 \;\; 40]$ mm.

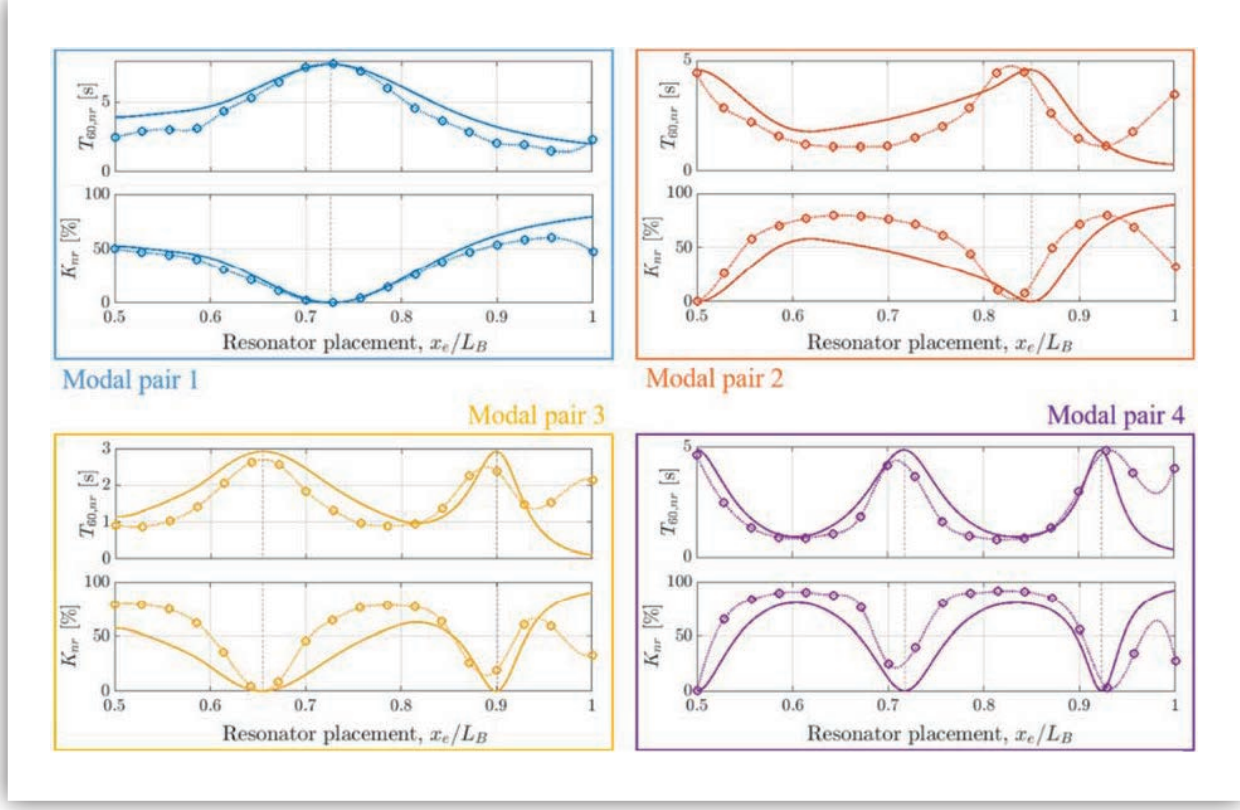

Figure 6. Variation of the decay time $T_{60,nr}$ (s) and resonator dissipation K_{nr} (%) as a function of the resonator placement x_e, for all four modal-pairs. The distance was fixed at $d/a = 0.4$ and the tuning ratio $\omega_r/\omega_n \simeq 1$. The solid lines and circles show the modelling and experimental results, respectively. The vertical dotted lines indicate the location of the nodal points in the bar modes.

4. Conclusions

In this paper we have developed a vibro-acoustic model describing the coupling dynamics between a vibrating beam and an acoustic resonator, as found in mallet percussion instruments like the marimba or the vibraphone. The bar is modelled as a free-free beam and the resonator as a cylindrical pipe, both in a modal framework. The vibro-acoustic coupling of the two elements was pursued assuming that only the circular region on the bar just above the resonator will interact with the resonator. The vibro-acoustic transfer function between two parallel disks was used, as developed and validated in a previous work [10]. The proposed formulation led to a simple multi-modal model describing a set of mechanical oscillators (beam modes) inertially coupled to a set of acoustic oscillators (resonator modes).

Experiments were carried out to validate various aspects of the proposed model: (1) the tuning ratio ω_r/ω_n, (2) bar-resonator distance d and (3) resonator placement along the bar length x_e. Despite some minor quantitative deviations, the vibro-acoustic model was positively validated by experiments, showing the often-encountered compromise between a decrease of decay time and an increase of acoustic radiation. Additionally, experiments showed that the coupling strength will be severely influence by the bar mode shape at the location where the resonator is placed $\psi_n(x_e)$, i.e. a resonator will not couple with a particular bar mode if it placed directly under a nodal line.

The simplicity of the developed lumped-parameter formulation allows for an intuitive understanding of the physical phenomena occurring in real instruments and underlines the main parameters affecting its dynamics. This can be a valuable contribution to the design and optimization of modern instruments, especially in the advent of instruments where multiple bar modes are tuned to multiple resonator modes, leading to increased sound radiation at several frequencies.

5. Acknowledgments

The authors gratefully acknowledge the financial support given by “Fundação para a Ciência e Tecnologia” (FCT – Portugal) through the PhD grant referenced SFRH/BD/140598/2018. Moreover, the authors would like to thank Prof. José Bento Coelho and Alexandre Pereira from the Centro de Análise e Processamento de Sinais (CAPS) at Instituto Superior Técnico for the access and support at the anechoic chamber.

6. References

[1] L. Henrique e J. Antunes, "Optimal design and physical modelling of mallet percussion instruments," *Acta Acustica,* vol. 89, pp. 948-963, 2003.

[2] F. Orduña-Bustamante, "Nonuniform beams with harmonically related overtones for use in percussion instruments," *Journal of the Acoustical Society of America,* vol. 90, nº 6, pp. 2935-2941, 1991.

[3] F. Soares, J. Antunes e V. Debut, "Multi-modal tuning of vibrating bars with simplified undercuts using an evolutionary optimization algorithm," *Applied Acoustics,* vol. 173, 2020.

[4] J. Petrolito e K. A. Legge, "Optimal undercuts for the tuning of percussive beams," *Journal of the Acoustical Society of America,* vol. 102, nº 4, pp. 2432-2436, 1997.

[5] D. Beaton e G. Scavone, "Three-dimensional tuning of idiophone bar modes via finite element analysis," *Journal of the Acoustical Society of America,* vol. 149, nº 6, pp. 3758-3768, 2021.

[6] F. Soares, J. Antunes e V. Debut, "Tuning of bending and torsional modes of bars used in mallet percussion instruments," *Journal of the Acoustic Society of America,* vol. 150, nº 4, pp. 2757-2769, 2021.

[7] I. Bork, "Practical tuning of xylophone bars and resonators," *Applied Acoustics,* vol. 46, pp. 103-127, 1995.

[8] P. Rucz, M. Á. Ulveczki, J. Angster e A. Miklós, "Simulation of mallet percussion instruments by a coupled modal vibroacoustic finite element method," *Journal of the Acoustical Society of America,* vol. 149, nº 5, pp. 3200-3212, 2021.

[9] F. Soares, J. Antunes e V. Debut, "Simplified model for the bar-resonator vibro-acoustic interaction in mallet percussion instruments," em *16e Congrès Acoustique Français*, Marseille, 2022.

[10] F. Soares, J. Antunes e V. Debut, "A minimal model of the bar-resonator vibroacoustic interaction in mallet percussion instruments," *Applied Acoustics (submitted Feb 2022).*

[11] F. Fahy, "Some applications of the reciprocity principle in experimental vibro-acoustics," *Acoustical Physics,* vol. 49, nº 2, pp. 217-229, 2002.

[12] T. t. Wolde, "Reciprocity measurements in acoustical and mechano-acoustical systems: Review of theory and applications," *Acta Acustica united with Acustica,* vol. 96, pp. 1-13, 2010.

Índice de anunciantes

HBK
HOTTINGER BRÜEL & KJÆR

DISEÑADO PARA SU TRABAJO

Presentamos el sonómetro HBK 2255

El sonómetro HBK 2255 con Building Acoustics Partner se ha diseñado específicamente para realizar medidas de acústica de edificios. Se trata de instrumento ligero y robusto, para realizar mediciones más rápidas, fáciles e inteligentes.

Gracias a sus aplicaciones para dispositivo móvil y PC, nunca había sido tan sencillo hacer medidas y análisis acústicos avanzados... y documentarlos. Para más información, visite www.bksv.com/2255.

HBM

Brüel & Kjær